

Extended Polarimetric Observations of Chaff using the WSR-88D Weather Radar Network

James M. Kurdzo, *Senior Member, IEEE*, Betty J. Bennett, John Y. N. Cho, and Michael F. Donovan

Abstract—Military chaff is a metallic, fibrous radar countermeasure that is released by aircraft and rockets for diversion and masking of targets. It is often released across the United States for training purposes, and, due to its resonant cut lengths, is often observed on the S-band Weather Surveillance Radar – 1988 Doppler (WSR-88D) network. Efforts to identify and characterize chaff and other non-meteorological targets algorithmically require a statistical understanding of the targets. Previous studies of chaff characteristics have provided important information that has proven to be useful for algorithmic development. However, recent changes to the WSR-88D processing suite have allowed for a vastly extended range of differential reflectivity, a prime topic of previous studies on chaff using weather radar. Motivated by these changes, a new dataset of 2.8 million range gates of chaff from 267 cases across the United States is analyzed. With a better spatiotemporal representation of cases compared to previous studies, new analyses of height dependence, as well as changes in statistics by volume coverage pattern are examined, along with an investigation of the new “full” range of differential reflectivity. A discussion of how these findings are being used in WSR-88D algorithm development is presented, specifically with a focus on machine learning and separation of different target types.

Index Terms—Weather radar, polarimetry, chaff.

I. INTRODUCTION

CHAFF, a military radar countermeasure that consists of metallic fibers cut to specific resonant frequencies, is used to mask aircraft, ships, and missiles from enemy detection [1]. While typically used operationally in the battlefield, chaff releases are common in United States airspace, likely for testing and training purposes (e.g., [2]). Given observations of chaff lengths ranging from 1–20 cm on the ground following releases [2], these metallic dipoles resonate at frequencies easily detectable by the 10-cm wavelength Weather Surveillance Radar – 1988 Doppler (WSR-88D) network across the United States [3], [4]. An example of chaff fibers and clumps is shown in Fig. 1 (from [5]).

Chaff is an air motion tracer, meaning that it often flows with the underlying atmospheric velocity field [6]–[11]. While this can theoretically be useful to users of weather radars, chaff is generally considered clutter for these systems [12]–[14]. In many cases, chaff can be nearly co-located with convective storms, and can take on an appearance that makes it exceptionally difficult to differentiate from weather. This is especially true for radar users that are either inexperienced or do not have access to polarimetric radar variables, which can greatly aid in differentiating between clutter and weather. As an example, air traffic controllers fall into the latter category,

since their displays primarily offer horizontal reflectivity factor (Z_H) and not polarimetric data [15]. An example of chaff mixed with weather is shown in Fig. 2. The areas of chaff are nearly impossible to identify by Z_H alone, but become discernible in the polarimetric fields, especially differential phase (ϕ_{DP}).

As part of efforts to characterize chaff and sea clutter (another clutter target for weather radar), several statistical properties of chaff have been examined across hundreds of cases for use in machine learning (ML) classification algorithms. These properties include Z_H , differential reflectivity (Z_{DR}), co-polar correlation coefficient (ρ_{HV}), and ϕ_{DP} . Statistical chaff characteristics were first presented by [16], but only one case in central Oklahoma was examined, leading to a long-held belief that chaff primarily presented only as horizontally oriented fibers, leading to mostly positive Z_{DR} . However, [5] showed more-detailed statistics covering 2.2 million range gates of chaff data, resulting in a deeper understanding of negative Z_{DR} in chaff, how often it occurs, and a theoretical basis for why it occurs.



Fig. 1. Chaff of various cut lengths (from [5]).

The motivation for this study is an upgrade to the WSR-88D that expanded the available Z_{DR} range from $-7.9 - 7.9$ dB to $-13 - 20$ dB. Since a large focus of [5] was on new observations of Z_{DR} in chaff, it is important to characterize Z_{DR} with the new, expanded scale. While exploring these data in a new, approximately 2.8-million range gate dataset collected in 2022, several additional statistical characteristics in chaff that were not covered in [5] were discovered. Additionally, through the development of an upgraded/combined

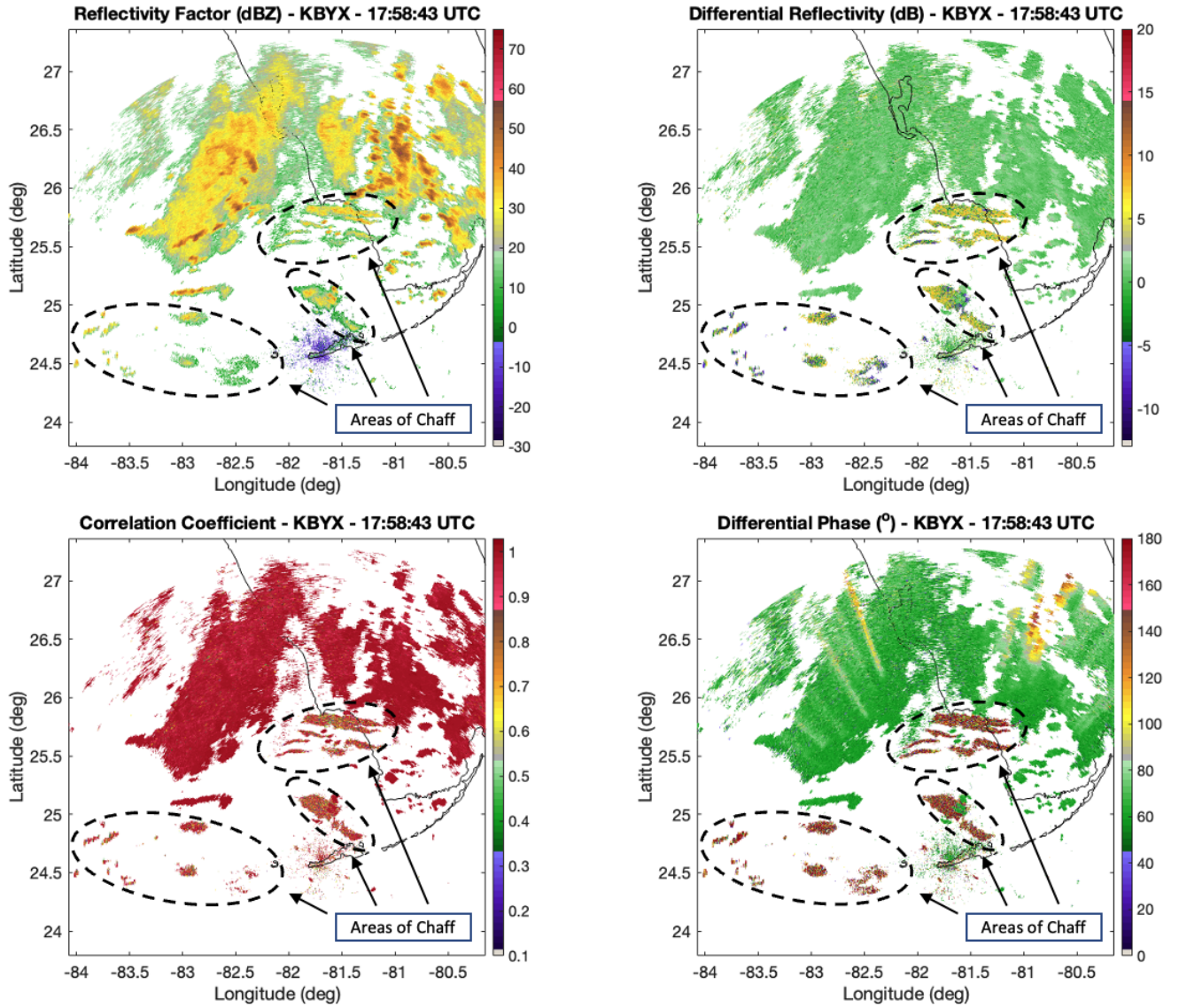


Fig. 2. An example case of chaff mixed with convection from the KBYX (Key West, FL) WSR-88D on 8 August 2016. Clockwise from the top left are horizontal reflectivity factor (Z_H), differential reflectivity (Z_{DR}), differential phase (ϕ_{DP}), and co-polar correlation coefficient (ρ_{HV})

sea clutter and chaff detection algorithm, it was found that the currently operational chaff detection algorithm (CDA) [17] with accuracy of approximately 80% was able to be improved to nearly 95% accuracy with the statistics gleaned from this new database when combined with similar data collection of sea clutter cases [18]. This paper focuses not only on the newly observed Z_{DR} statistics, but also on new observations of other parameters.

This paper is designed to build upon, and augment, [5] for use as a training tool for weather radar users across the weather enterprise. In addition, ongoing efforts to detect and differentiate chaff and sea clutter [17] can heavily benefit from these new statistics. Use of the expanded Z_{DR} data, as well as discussions of Z_H and vertical reflectivity factor (Z_V) dependence on height, an approximation of circular depolarization ratio (pseudo circular depolarization ratio; $PCDR$), and different Z_H and Z_{DR} characteristics by WSR-88D vol-

ume coverage patterns (VCPs) discussed in this paper will be beneficial to ML algorithms currently under development to discriminate chaff and sea clutter from weather, ground clutter, and biological scatterers. Although the paper is focused on data from the WSR-88D network, it is anticipated that the methods and application to ML algorithms will be useful for other radar systems and networks around the world.

The paper is organized as follows: the data, methods, and description of polarimetric weather radar variables are first discussed. Next, statistical observations of chaff across the entire dataset are presented. Finally, a discussion of the findings and conclusions is provided.

II. DATASET

The dataset used in this study was collected during an intensive observation period from January – June 2022 and

includes 267 cases (including all tilts from each case) and approximately 2.8 million individual range gates of chaff. A “tilt” is a constant-elevation-angle scan, otherwise known as a plan position indicator (PPI). A “case” is defined as a single volumetric scan at a single point of time from one radar site during a chaff “event.” Events are defined as an entire chaff release episode, which can sometimes last over 12 hours. Cases of chaff sometimes exist from separate radar sites at a similar time to another radar site(s), but, in most cases, only one time per event per radar is included in the database. A small number of events (fewer than 10) contain two cases that are at least 8 hours apart due to significant changes in chaff structure and statistics over a long-duration release. This means that, for the majority of events, the dataset does not contain multiple volumes from the same radar in the same event, making the database spatiotemporally diverse, especially compared to [5]. In [5], some cases were from similar times within the same event and from the same radar. Additionally, in the present dataset, there is a significant increase in the diversity across radar sites spatially. Cases from 71 sites across the CONUS are included, with the most from one radar being 32 from KNKX (San Diego, CA).

It should be noted that despite the much larger number of cases in this paper compared to [5] (267 versus 75), only a modest increase in the number of range gates used for analysis is realized (2.8 million versus 2.2 million). This is due to the fact that a wider range of sites and “types” of cases were included in the dataset. In [5], many of the cases were relatively large spatially since they were straightforward to identify. The currently operational CDA was developed with the statistics from [5] and operationalized on the WSR-88D in 2021 [17]. This algorithm was used only to *identify* cases across the entire WSR-88D fleet, including smaller spatiotemporal cases with varying statistics. It is important to note that while the existing CDA was used to identify *possible* cases, all data in this study were collected manually via the description below. No automation of case selection was used.

The spatial distribution of sites and the temporal distribution across six months in the present dataset makes it an arguably better representation of chaff characteristics across the CONUS than that in [5], while also including the added Z_{DR} range, discussion of Z_V , new $PCDR$ calculations, and separation by height and VCP. All statistics are calculated using the Open Radar Product Generator Simulator (ORPGSim), a MATLAB clone of the operational WSR-88D ORPG. ORPGSim provides nearly identical results to the operational ORPG for generating products, but offers the flexibility of simplified processing and workflows for collection and analysis of large amounts of data. As part of this software package, a region-of-interest tool was used to manually truth range gates of chaff using a subject matter expert-defined polygon drawn around clusters of chaff at each tilt within a volume. A description of this collection technique is detailed in Section 2c of [5]. Every tilt of every case was manually truthed by a human, and the associated masks were used to isolate chaff range gates. It should be noted that there is no *actual* ground truth of chaff in any of our cases (i.e., no definitive proof that what we are seeing is indeed chaff). The

only known case with literal ground truth was presented in [2], where chaff was found on the ground after a very concentrated chaff release. Our approach is based on the fact that no other known target type displays these signatures, and the signatures that serve as our “truth” are relatively well-accepted in the broader literature.

In order to further refine the chosen range gates, all ρ_{HV} values ≥ 0.97 were removed from the final dataset. Additionally, all range gates with a standard deviation of ϕ_{DP} less than 10° were removed. The standard deviation of ϕ_{DP} in this context is an ORPG-defined product that uses unwrapped ϕ_{DP} values. This is a different approach from [5], and is meant to remove range gates of chaff that are mixed with, and dominated by, weather. The values chosen for censoring are based on the fuzzy logic membership functions in the Inanimate class of the Hydrometeor Classification Algorithm (HCA; [19]) discussed in [20]. These values were originally determined using a genetic algorithm to optimize the membership functions using a series of chaff, sea clutter, and ground clutter cases. They were found to be the optimal combination of parameters to identify these target types and avoid categorizing weather and other clutter as chaff or sea clutter. These more-stringent restrictions also account for a non-trivial decrease in the number of range gates in the database used for analysis.

Similar to [5], an unfolded “full” ϕ_{DP} product was mimicked in ORPGSim, allowing ϕ_{DP} values up to 360° . Values 60° and below were not used due to the system initial phase generally being set to 60° , resulting in a large spike where ϕ_{DP} values at or below 60° are cut off. This invariably misses some folded ϕ_{DP} values, but the number of range gates that fit into this category is exceptionally low. For height calculations, a standard $4/3$ Earth’s radius model is used to calculate the beam height at each range gate based on range and elevation angle [21].

In addition to the aforementioned radar variables (Z_H , Z_{DR} , ρ_{HV} , ϕ_{DP}), also presented in [5], this study also discusses Z_V , Doppler spectrum width (W), and $PCDR$. The formulation used for $PCDR$ is an approximation of the circular depolarization ratio (CDR) for simultaneous transmission/reception of horizontal/vertical polarization (SHV) radars defined in [22]:

$$PCDR = \frac{1 + Z_{DR}^{-1} - 2\rho_{HV}Z_{DR}^{-1/2}}{1 + Z_{DR}^{-1} + 2\rho_{HV}Z_{DR}^{-1/2}} \quad (1)$$

It is important to note that in this study, the inputs of Z_{DR} and ρ_{HV} to (1) are in derived product form, as with the rest of the analyzed data. Within the WSR-88D processing scheme, derived products consist of post-processed “products” that are outputs from the ORPG; derived products are the input source to most downstream ORPG algorithms such as the HCA. The primary derived products are modified versions of the base radar variable estimates, including processing such as recombination from 0.5° to 1.0° and other data quality assurance measures.

CDR has been shown to be useful for discriminating between meteorological and non-meteorological targets [22]–

[26] and, most relevantly to this study, between hydrometeors and chaff [9]. Given that it is not a “native” variable in SHV radars, it is rarely used operationally [22] and is an unused tool in algorithmic development on the WSR-88D. Although [27] showed that CDR can be expressed in terms of linearly polarized radar parameters, [9] noted that this formulation is quite sensitive to propagation effects, and instead proposed $PCDR$ (or what they called depolarization ratio), which is more robust against propagation effects. With work underway to differentiate chaff from other target types, a discussion of $PCDR$ and its relation to other variables of interest is considered warranted in this study.

III. STATISTICAL OBSERVATIONS

This section focuses on the broad statistical properties of chaff within the newly collected dataset from 2022. A deeper discussion on selected topics is presented in the following section. For each figure shown, all 2.8 million range gates across all 267 cases are included in the histograms. Direct comparisons are made with the dataset in [5] when appropriate.

Histograms of Z_H , W , ρ_{HV} , and ϕ_{DP} are shown in Fig. 3. Z_H shows a roughly Gaussian shape centered just below 10 dBZ. The observed distribution differs from the “plateau” seen in Fig. 3 of [5], but is centered in a similar range. The higher concentration of values from -10 dBZ – 10 dBZ is thought to be due to the addition of more cases with varying spatial extents. As opposed to the dataset in [5], which chose cases that were often at their peak spatial extent (i.e., the most easily identifiable cases), the present dataset includes a much-higher number of cases that have relatively small spatial footprints, both vertically and horizontally. Anecdotally, through extensive data collection and observation, cases with smaller chaff cloud sizes tend to have lower reflectivity, which lends credence to the observed histogram.

The histogram of W was not included in [5], but is shown here due to its importance in the work from [20], which utilized statistics from [5] to develop a new hydrometeor class (called “Inanimate”) for the WSR-88D HCA. It was found in [20] that exceptionally low values of W were present in all of the target types encompassed by the Inanimate class, which include chaff, sea clutter, combustion debris, and radio frequency interference. However, in recent attempts to separate chaff from sea clutter, there are distinct differences in the peak and tail of W , making these findings relevant at the current time. It makes intuitive sense that chaff would have a low W distribution since most cases collected did not overlap with convective storm cells where high W values can be expected. Increased values of W do seem to be present in cases of chaff near or adjacent to convection (not shown), but the tail drops off quickly after 3 – 4 m/s. It should be noted that *most* cases in the database consist of chaff-only scatterers, so the true values in the W histogram may extend slightly higher in cases where chaff is mixed with convective weather. However, in most cases, the dominant scatterer (be it chaff or weather) is what is “detected” by the radar. Of course, if chaff is detectable but mixed with weather, we would expect to see elevated W estimates.

In ρ_{HV} and ϕ_{DP} , the distributions are largely similar to those shown in [5]. The differences are that ρ_{HV} values greater than or equal to 0.97 were discarded in this dataset due to the proximity of weather in some cases, and values of ϕ_{DP} less than or equal to 60° were discarded due to the setting of system initial phase. Range gates where the standard deviation of ϕ_{DP} was less than or equal to 10° were also discarded, which slightly alters the ϕ_{DP} distribution. The standard deviation of ϕ_{DP} was calculated in the identical fashion to the ORPG, which creates a “hidden” product that is part of the operational HCA. This product is what is referred to as a texture field in [19], which is calculated using a comparison between a sliding smoothing window and the original data. The exact filter values are detailed in [19].

For ρ_{HV} , a peak near 0.5 with a relatively sharp dropoff toward 0.1 is seen. A much more muted drop in distribution of ρ_{HV} is seen towards the highest values at 0.96. It should be noted that, as in [5], there are cases of chaff range gates that extend to the maximum ρ_{HV} estimate of 1.03, but they were discarded for this dataset. Note that in the WSR-88D processing of derived products, some ρ_{HV} estimates can be as high as 1.03. These values were clipped and removed in the histograms. For ϕ_{DP} , as with the dataset in [5], a peak around $100 - 120^\circ$ is seen, with a gradual dropoff toward 200° and a long tail to 360° . Unlike Fig. 3 in [5], folded values that end up below 60° are not included.

Typically, ϕ_{DP} is not a tool directly used in weather radar analysis; rather, its path derivative, specific differential phase (K_{DP}), is used. However, in many dual-polarimetric weather radars, the WSR-88D included, K_{DP} is not calculated for ρ_{HV} values under a given value (0.9 for the WSR-88D) due to the unlikelihood that rain is present. Therefore, on many radars, K_{DP} is not calculated in instances of chaff. It turns out that ϕ_{DP} is itself very useful for identifying chaff due to its highly stochastic nature compared with the relatively smooth gradients seen in weather (as seen in Fig. 2). This appearance is due to the fact that chaff, if treated as a dipole, has zero differential backscatter phase. The combination of receiver differential phase as the primary contributor and high measurement error due to very low cross-correlation coefficients [16] makes for this hallmark stochastic presentation in ϕ_{DP} [5]. In cases when the standard deviation of ϕ_{DP} is less than 10° , we have seen, both qualitatively and quantitatively, that chaff is exceptionally unlikely to be present, *or*, weather is the dominant scatterer in the resolution volume.

With the latest software processing upgrades to the WSR-88D (as of late 2021), every case in the present 2022 dataset is able to provide Z_{DR} information between -13 – 20 dB. Previously, values that fell beyond -7.9 – 7.9 dB were clipped. In [5], those clipped values were eliminated. In Fig. 4, the full range of Z_{DR} is shown with the dashed vertical black lines indicating the previous -7.9 – 7.9 dB Z_{DR} range. Within the previous range, the distribution is a bit different than that seen in [5]. A more plateaued shape is seen in the 2022 dataset, with relatively flat probability densities between 0 and 5 dB. In [5], there was a peak around 1.5 dB and a slow dropoff toward the 7.9 dB limit, while here, the peak is at 4 dB. The relatively plateaued shape is in stark contrast to the sharper

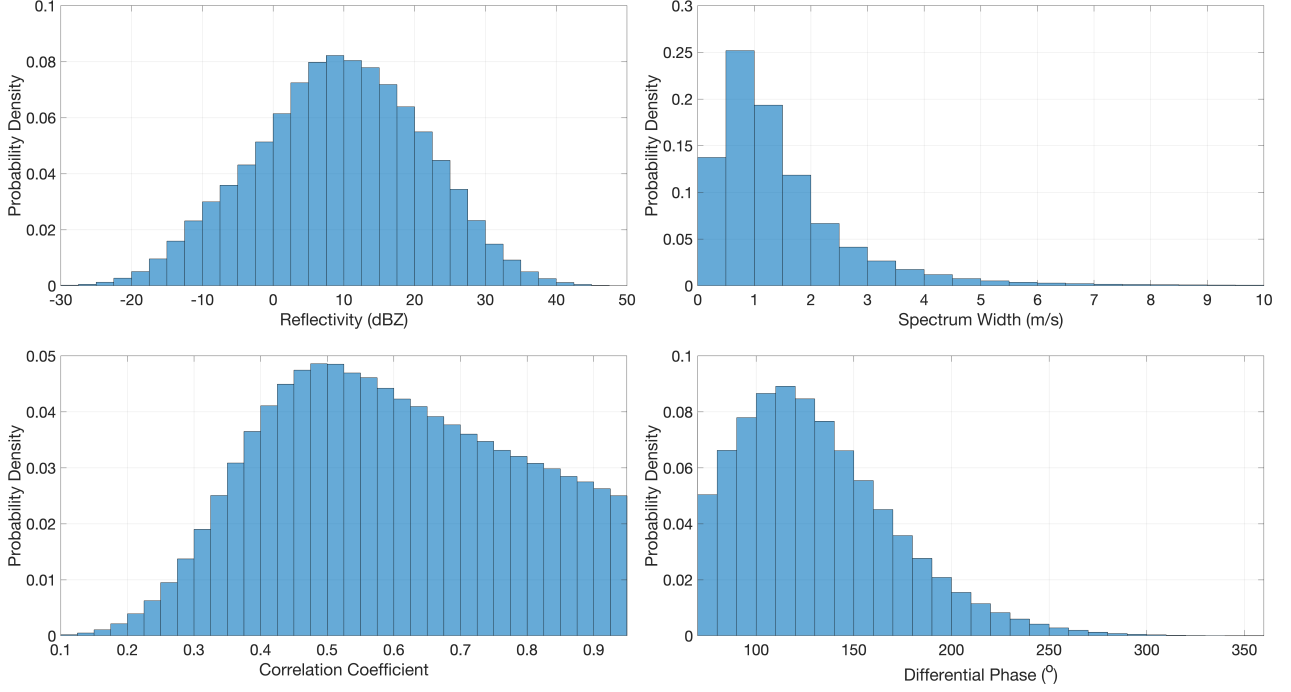


Fig. 3. Histograms of approximately 2.8 million range gates of chaff from 267 cases. From top left, counterclockwise: horizontal reflectivity factor (Z_H), spectrum width (W), differential phase (ϕ_{DP}), and co-polar correlation coefficient (ρ_{HV}).

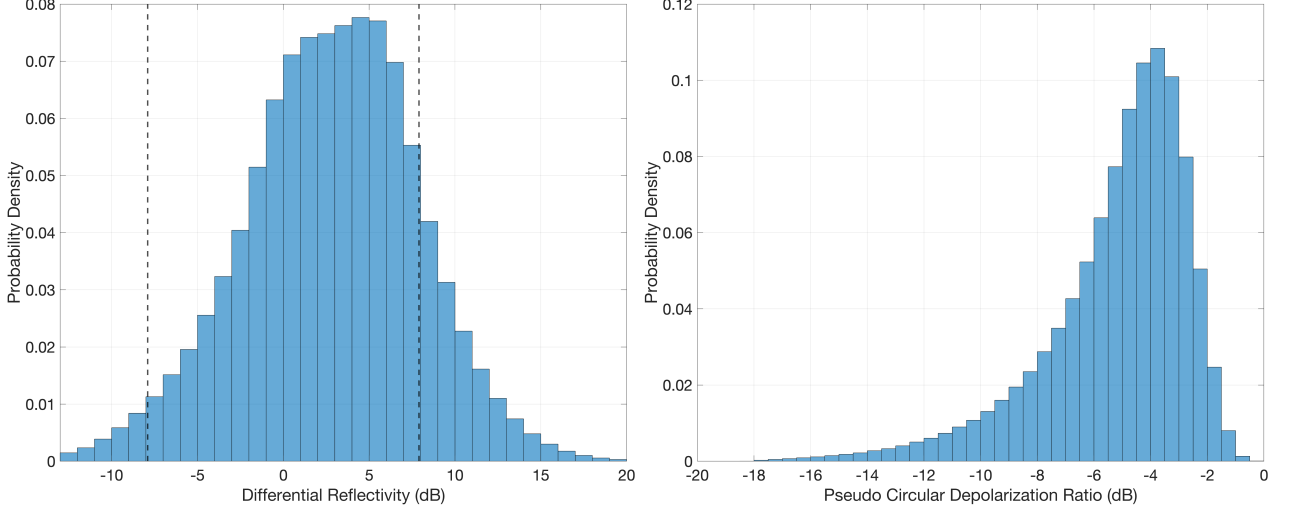


Fig. 4. Histograms of approximately 2.8 million range gates of chaff from 267 cases. Left: differential reflectivity (Z_{DR}); right: pseudo circular depolarization ratio ($PCDR$) from [22]. Vertical dashed black lines indicate the previous Z_{DR} range of $-7.9 - 7.9$ dB.

peak at 1.5 dB in [5], demonstrating a consistent distribution of Z_{DR} values between roughly 0 – 5 dB. This observation of a shift toward higher Z_{DR} values is thought to be indicative of a more-diverse dataset in the present study. For example, with a wider spatial range of data (i.e., more sites across the country), different types of chaff may be used, leading to a possible shift in distribution. However, it is not completely clear why this shift is seen in the 2022 data.

In Fig. 4, the dropoff after 5 dB is sharp and rapid, decreasing by nearly a factor of two before reaching 8 dB. However, most importantly, a non-trivial percentage of the distribution (17%) is observed outside of the original bounds. This is particularly true on the positive side ranging from 7.9 – 20 dB. A total of nearly 15% of all chaff range gates fall above 7.9 dB. Additionally, a small tail also extends from -13 – -7.9 dB, showing additional information gleaned for strongly

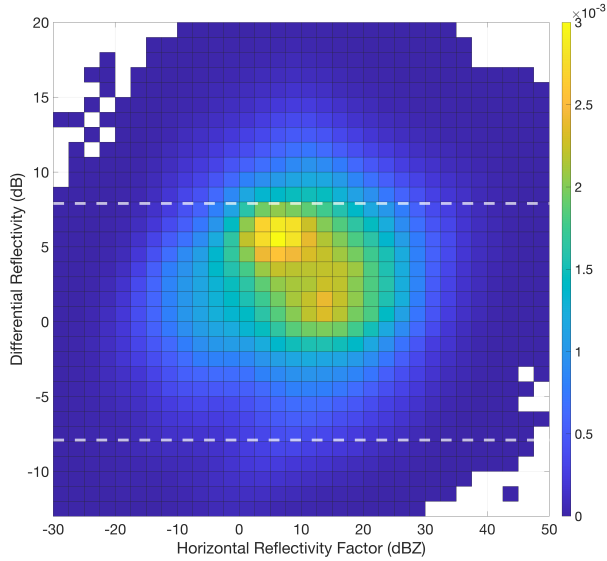


Fig. 5. Distribution of chaff range gates between horizontal reflectivity factor (Z_H) and differential reflectivity (Z_{DR}). Horizontal dashed white lines indicate the previous Z_{DR} range of $-7.9 - 7.9$ dB.

vertically oriented fibers with the new Z_{DR} range.

It should be noted that Z_{DR} calibration is a known issue with the WSR-88D system [28], leading to biases that can sometimes exceed ± 0.5 dB [29]. While these biases can be monitored using techniques such as Bragg scatter detection, they are not recorded as a definitive value in WSR-88D data (and can change over even short periods of time) [29]. Since correcting for Z_{DR} biases is impractical for this study, it is assumed that the biases are small enough to still get the general trend of Z_{DR} values. It is also important to consider that the distribution of Z_{DR} values in this study represent the data used to train the updated CDA in [18]. This generally favors algorithm performance, since calibration is not accounted for in real-time data streaming either (i.e., as data are fed to the algorithm for processing and display).

The distribution of $PCDR$, calculated using the approximation from [22] shown in (1), has not been explored before in a large number of chaff cases. Several studies have shown various types of clutter to fall within the range of $-10 - -1$ dB, while weather is generally much more negative [22], since spherical particles reflect much more strongly in the opposite circular polarization sense than in the same sense. In Fig. 4, the $PCDR$ histogram fits this expectation, with a peak close to -4 dB, a sharp dropoff to -1 dB, and a long tail out to approximately -18 dB. Further discussion on these findings and their importance to algorithmic development is provided in the next section.

Given the advent of a new range for Z_{DR} , it was prudent to compare Z_H versus Z_{DR} in a similar fashion to Fig. 5 from [5]. The results are shown in Fig. 5, with Z_H along the abscissa and Z_{DR} along the ordinate. Similar to the differences in Z_H distribution between Fig. 3 and [5], the distribution in Fig. 5 is skewed toward lower Z_H values compared to [5]. Additionally, the plateaued nature of the Z_{DR} distribution

in Fig. 4 is evident in Fig. 5. When combined, there is a range of distinct hot spots from 5 dBZ / 5 dB (for Z_H and Z_{DR} respectively) to 15 dBZ / 0 dB (also for Z_H and Z_{DR} respectively). While this is not surprising given the histograms in Figs. 3 and 4, two additional interesting features are apparent. First, at Z_{DR} values beyond 7.9 dB, the Z_H values tend to sit between 0 and 20 dB. This indicates that the extension of Z_{DR} to higher values correlates with a wide range of Z_H values.

In [5], the only examples of height dependence were presented for Z_{DR} and were focused on individual case studies. Violin plots were shown for several ranges of heights spanning eight different case studies. Z_{DR} was also explored temporally throughout the lifetime of a chaff cloud's fallout for the same eight cases. However, no holistic view of Z_{DR} with height was explored, and no statistics of Z_H were discussed in a spatiotemporal sense. In Fig. 6, the dependence of Z_H , Z_V , Z_{DR} , and $PCDR$ with height are shown. Both Z_H and Z_V show trends of increasing with height, although Z_V peaks at slightly lower values at a similar height as Z_H (roughly 750 m above radar level). A discussion on this effect and what it implies for algorithm development is provided in the following section.

Also in Fig. 6, the dependence of Z_{DR} on height is shown. In general, the Z_{DR} distribution above 250 m stays relatively similar with height, mostly matching the histogram in Fig. 4 and agreeing with what would be expected from the Z_H and Z_V distributions in the top row of Fig. 6. However, a negative shift in distribution is apparent at lower heights, which would agree well with the case studies in [5] where Z_{DR} values close to zero were seen at the lowest levels and Z_{DR} values between $3 - 6$ dB were more common at higher elevations. Finally, $PCDR$ displays a relatively consistent distribution with height, with a strong focus around -3 to -4 dB. There appears to be a slight decrease in $PCDR$ with height, near -0.5 dB per km between 250 m and 2 km. Additional discussion on these observations follows in the next section.

Finally, differences were noted in the database when comparing statistics between different VCPs. VCPs are defined by the scan pattern of the radar, including (but not limited to) the number/exact value of tilts, pulse repetition frequency, and scan rate. In general, precipitation VCPs have more tilts but scan at higher rates, resulting in both faster volumetric and single-elevation update rates. Despite their name, clear air VCPs are often used in cases of light stratiform precipitation, especially snow. VCP 31, a clear air VCP, is a unique scanning mode for the WSR-88D in that it is the only VCP that uses a longer pulse ($4.7 \mu s$) than the other VCPs ($1.57 \mu s$).

In order to investigate these observations, each range gate within each case was separated into the current VCP at the time of the case. Histograms of Z_H for two sets of VCP combinations are detailed in Fig. 7: precipitation versus clear air VCPs. In Fig. 7, the clear air VCPs show a much lower peak Z_H value in their distribution relative to the precipitation VCPs. The precipitation VCPs are centered nearly 10 dBZ higher than the clear air VCPs, but have a long, low tail out to -30 dBZ (compared with a more-gradual falloff at low Z_H values in the clear air VCPs). Thoughts behind these

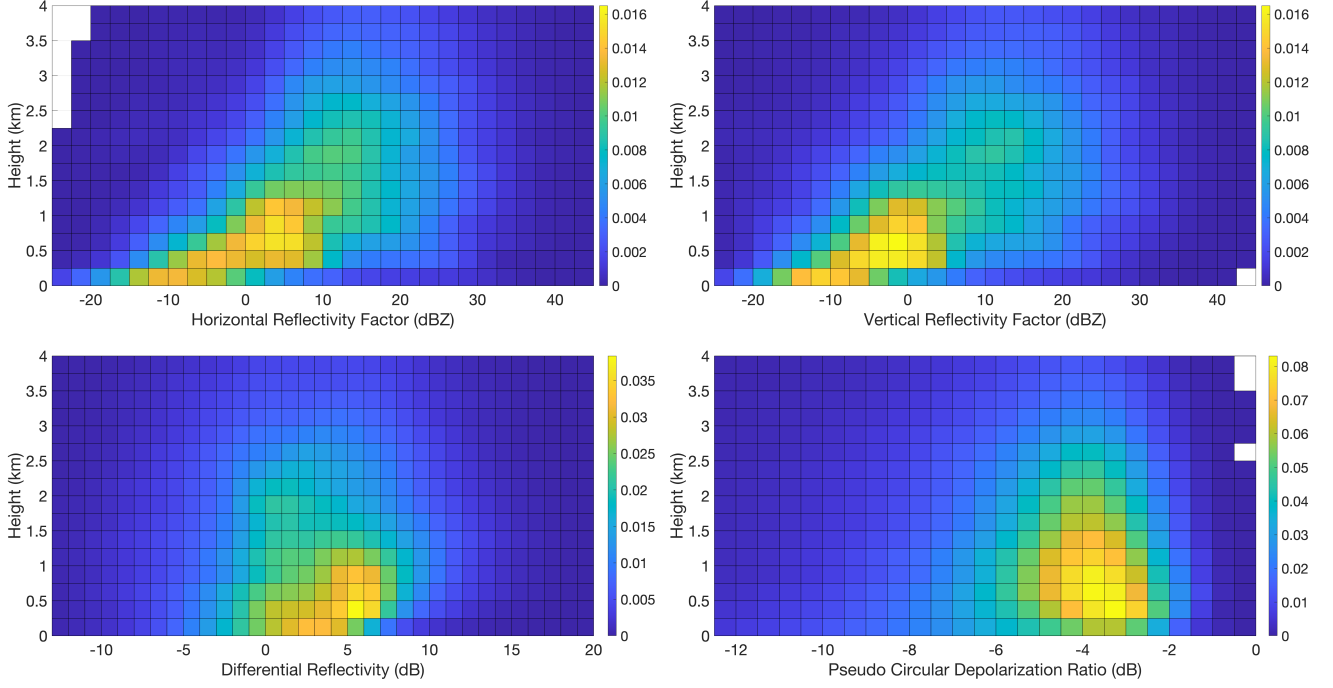


Fig. 6. Height-based chaff distribution of horizontal and vertical reflectivity factors (Z_H and Z_V ; top row, from left to right), as well as differential reflectivity and pseudo circular depolarization ratio (Z_{DR} and $PCDR$; bottom row, from left to right). Heights are relative to the radar's elevation.

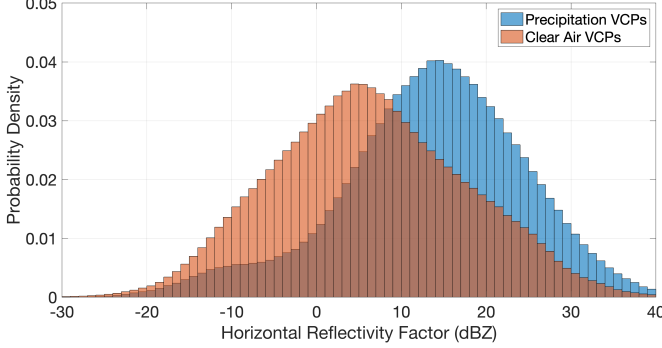


Fig. 7. Histograms of chaff horizontal reflectivity factor (Z_H) broken out by precipitation and clear air volume coverage patterns (VCPs).

observations are offered in the following section.

IV. DISCUSSION

A more-detailed discussion of three selected statistics is provided in this section, including the distribution of $PCDR$, observations of Z_H , Z_V , Z_{DR} , and $PCDR$ by height, and the distribution of Z_H and Z_{DR} broken out by VCP.

A. Depolarization Ratio Distribution

As chaff is considered an air motion tracer, and is most-often found in laminar airflow (i.e., not near convection), chaff is oriented horizontally *most* of the time (as evidenced in Fig. 4). It is known from [5] that there is a period of

time during chaff fallout, usually during the beginning, that features vertically oriented fibers, contributing to most of the negative Z_{DR} values in the histograms in both [5] and the present study. Additionally, as discussed in [16], the linear depolarization ratio (LDR) in chaff is expected to be relatively high compared to precipitation.

[16] assumed that the angle between the horizontal plane and the chaff axis was distributed uniformly between zero and a maximum angle called the flutter angle. With this approach, a flutter angle of zero corresponds to all chaff being horizontally oriented ($Z_{DR} = +\infty$), while a flutter angle of 90° corresponds to a uniform distribution of chaff orientation ($Z_{DR} = 0$ dB). Their Hertzian dipole model using LDR (their Fig. 3) showed that LDR values are asymptotic approaching just above -5 dB as the flutter angle approaches 90° . In fact, the model only dips to about -10 dB at a flutter angle of 30° , which corresponds to an approximate Z_{DR} of 15 dB. This suggests that, in the presence of chaff, it would be expected to see values of LDR between -10 and -5 dB, but more extremely horizontally oriented chaff could dip to lower LDR values (-13 dB for a Z_{DR} value of 20 dB). However, LDR cannot be measured by a radar operating in SHV mode, like the WSR-88D. Thus, we consider the use of CDR instead, which can be approximated using SHV-derived variables via the $PCDR$ formulation.

For a radar operating in circular polarization mode, the CDR is the received cross-polarized power divided by the co-polarized power. CDR is expected to be an excellent discriminator between hydrometeors and chaff because a perfect sphere reflects all signal in cross-polarized form (CDR of

$+\infty$), whereas a resonant dipole (an approximation of a chaff strand) has a CDR of 1 (0 dB). In reality, hydrometeors are not perfect spheres and chaff strands are not perfect dipoles, but the CDR for chaff is still typically expected to be (and has been observed to be) about 20 dB greater than the CDR for most hydrometeors [9].

Radars that operate with SHV-polarized signals cannot directly measure CDR . Although [27] showed that CDR can be expressed in terms of linearly polarized radar parameters, [22] noted that this formulation is quite sensitive to propagation effects, and instead proposed the $PCDR$ approximation, or what they called depolarization ratio (DR), that is more robust against propagation effects. $PCDR$, which is expressed via (1), is computed from the measured SHV parameters that can be written as

$$Z_{DR} = \frac{\langle |s_{hh}|^2 \rangle}{\langle |s_{vv}|^2 \rangle} \quad (2)$$

and

$$\rho_{HV} = \frac{\langle s_{hh}^* s_{vv} \rangle}{\sqrt{\langle |s_{hh}|^2 \rangle \langle |s_{vv}|^2 \rangle}}, \quad (3)$$

where s_{hh} and s_{vv} are scattering coefficients for the horizontal and vertical polarizations, respectively, and the asterisk denotes complex conjugation.

Would $PCDR$ be as good a discriminator between hydrometeors and chaff as CDR ? For hydrometeors, [22] showed $PCDR$ to be generally less than -15 dB. For chaff, one would expect $PCDR$ to be close to the theoretical 0 dB for CDR , but it is not immediately obvious from (1) that this would be the case. Z_{DR} and ρ_{HV} depend on the flutter angle of chaff [16]; although the Hertzian dipole model is only strictly valid for chaff lengths much shorter than the radar wavelength, [16] showed that its flutter angle dependency is very similar to a thin wire model. The simple dipole model is convenient, because a closed-form solution is available under reasonable assumptions. A derivation of this model is provided in the Appendix.

This is visually illustrated in Fig. 8, where the resulting dependency of $PCDR$ on the flutter angle is shown. It is clear that although $PCDR$ has a flutter angle dependency, the range is quite limited (-3.7 to 0 dB). Since hydrometeor $PCDR$ is expected to be generally less than -15 dB, this derived SHV parameter seems promising for separating chaff from hydrometeor signals. The $PCDR$ model result is substantially different than the LDR model in [16] in its limited range, but the histogram in Fig. 4 shows values much lower (as low as -18 dB) than the minimum values shown in Fig. 8 (approximately -3.7 dB). We must consider the fact that chaff is not a perfect dipole, is distributed in space, likely consists of inconsistent cut lengths, and can clump [5], meaning that we can expect lower values in real-life scenarios. Additionally, the model presented in (9) assumes a maximum flutter angle of 90° , meaning that the orientation can only reach an equal distribution between horizontal and vertical (i.e., Z_{DR} of 0

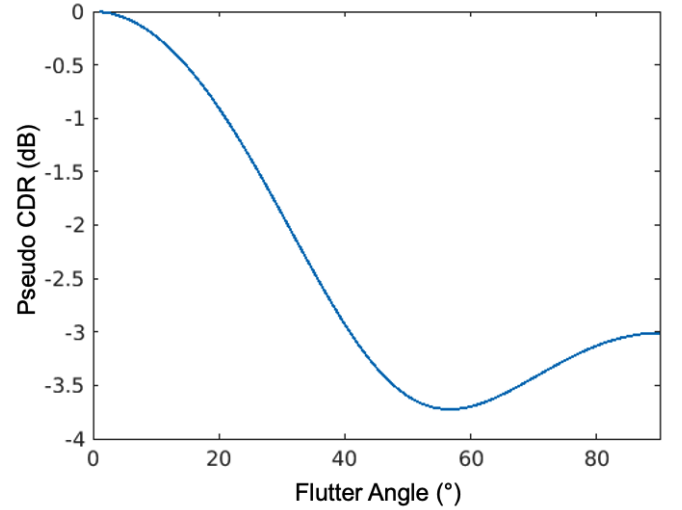


Fig. 8. $PCDR$ s for a dipole model based on flutter angle. Compared with the LDR results in [16], it is clear that the expected values of $PCDR$ are higher than LDR for a perfect dipole, even at extreme flutter angles. In fact, the entire range of $PCDR$ is only about 3.7 dB for the a dipole covering all flutter angles.

dB). If the chaff orientation distribution leans toward the vertical (i.e., negative Z_{DR}), the $PCDR$ values will extend lower than what is modeled in Fig. 8, likely partially contributing to the extended tail seen in Fig. 4.

In considering the utility of the distribution shown in Fig. 4, the measured distribution is still considerably narrower than that of hydrometeors, and the majority of the distribution is well above the expected range of hydrometeor $PCDR$ values [24]. This analysis suggests that an estimate of $PCDR$ can be useful for discrimination of chaff using advanced methods such as ML. While an ML algorithm could conceivably discern the different weights of importance of Z_{DR} and ρ_{HV} , especially in combination, between chaff and weather, feeding more-primitive ML algorithms a direct relation such as that provided in $PCDR$ may lead to a better/faster convergence on an acceptable classifier. Indeed, this has been seen in the recent ongoing development of a chaff detector, first presented in [17]. With the use of support vector machines, overall performance has been determined to increase in their approach by using a $PCDR$ estimate of WSR-88D data [18].

B. Height Dependence of Z_H , Z_V , Z_{DR} , and $PCDR$

Given the importance of driving a ML-based algorithm with relevant data that can lead to convergence on a better model more quickly, it is relevant to explore the spatial statistics of chaff. This is particularly relevant because spatial variables (range, height, etc.) are readily available in real-time processing, and any potential signal that can be derived using a large dataset could be simply included in a ML algorithm (both in training and operations). In order to identify these potential signals in the present dataset, four variables are examined by height: Z_H , Z_V , Z_{DR} , and $PCDR$. Relationships with range were also explored, but are not shown in this paper.

There is little reason to expect a *direct* dependence of chaff characteristics as a function of range alone (other than

a decrease in sensitivity), but there are three other spatially oriented aspects that could theoretically have impacts on what the radar estimates. These three aspects are height, resolution volume size (which is correlated with range), and elevation angle of the antenna. Height dependence could arguably be a physically viable expectation due primarily to the results in [5]. For example, different stages of chaff dispersal, as well as variations in the effect of the electric field (e.g., by height and/or by chaff cut length) could have impacts on statistical distributions. According to [5], chaff is often more likely to be vertically oriented at lower elevations due to the increasing strength of the fair weather electric field.

Resolution volume dependence could be viable because as the volume increases in size, it is less likely that chaff will meet the volume-filled scattering assumption in the calculation of reflectivity factor [21]. Finally, the elevation angle of the antenna could have an impact due to the fact that the “vertical” polarization of the radar becomes less truly vertical as the elevation angle increases. This is because as the antenna points at higher elevations, the angle of the vertical polarization becomes less orthogonal relative to the ground (becoming parallel to the ground when pointing to 90°).

In terms of viability, it seems unlikely that the impact of elevation angle would be significant with the WSR-88D due to the relatively low antenna pointing angles (up to 19.5° maximum, but focused mostly at lower angles, especially in clear air VCPs). It also seems unlikely that the resolution volume size is a meaningful factor, since we see the opposite effect in Fig. 6. That is, reflectivity increases with height rather than decreasing like we would expect if the resolution volumes were not being adequately filled to meet the reflectivity factor calculation assumption.

Therefore, we are left with exploring the impacts of height dependence based on different stages of fallout. The subplots in Fig. 6 allow for the exploration of these variations, including increasing Z_H and Z_V with height, increasing Z_{DR} with height, and a slightly decreasing $PCDR$ with height. When chaff is initially released, it appears in a relatively small footprint on the WSR-88D before dispersing with the prevailing atmospheric wind. This dispersion results in size sorting vertically [5], with clumps and vertically oriented fibers falling out prior to horizontally oriented fibers. Before widespread dispersion spatially, the concentration of chaff is at its highest point immediately post-release. Therefore, it makes intuitive sense that Z_H and Z_V would be at their highest values at higher heights (near release points), and decrease at lower elevations where the originally concentrated chaff has dispersed significantly due to the effects of differential advection (in the horizontal) and differential sedimentation (in the vertical). Since sedimentation only operates in one direction (downward), it makes sense that the further chaff gets from the height of release (further downward), the weaker the reflectivity factor will be on average.

Additionally, the results presented in [5] suggest that lower Z_{DR} values are likely at lower heights (due to the impact of the fair weather electric field), which agrees well with the Z_{DR} distribution seen in Fig. 6. This is because longer chaff strands are more-heavily impacted by the increasing electric

field strength closer to the Earth’s surface, causing them to tilt more vertically and hence fall out faster. An additional consideration not mentioned in [5] that has become evident in the current study is that there may be holistic effects on Z_{DR} as chaff descends into the planetary boundary layer (PBL). Turbulent mixing within the PBL may change the chaff orientation distribution from one that is (for example) mostly horizontal to a more isotropic distribution, which would shift the Z_{DR} distribution from positive values toward values closer to 0 dB near the Earth’s surface.

One concern regarding the suggested PBL impacts is that there may be unintended effects within the PBL in the chaff database. For example, if not carefully considered, chaff in the presence of other target types typically found within the PBL (clutter, insects, and other biota) could affect the statistics. The truthing mechanism used in this study mitigates this concern as much as possible. Given that each “cell” of chaff was manually traced using a region-of-interest polygon tool, it was determined by a subject matter expert that the gates being included were *dominated* by chaff. This is an important distinction, since clearly chaff can be mixed with other scatterers. In practice, if it was not exceedingly clear to the subject matter expert that the dominant scatterer was chaff, the case was not included in the database. While it is still possible that some biota and other targets are included, it is expected that the influence is exceptionally small.

Finally, the slight decrease in $PCDR$ is difficult to explain physically. The model depicted in Fig. 8 suggests that as the flutter angle decreases (a more horizontally oriented distribution), $PCDR$ *generally* increases. This would suggest that we should see increasing $PCDR$ with height since Z_{DR} is increasing with height. It should be considered that ρ_{HV} is not being taken into account when simply comparing against flutter angle (a ρ_{HV} dipole model is not shown in this paper). Additionally, as mentioned above, inconsistencies with chaff distribution, cut lengths, and clumps result in $PCDR$ values well outside the range predicted by the simplistic Hertzian dipole model. With these issues taken into account, it is not clear whether the shift in $PCDR$ with height is statistically meaningful or if there is even an underlying physical mechanism at play. A more-realistic model for $PCDR$ in chaff would be required to determine the answers to these questions, an endeavor that is beyond the scope of this paper. What is important in these findings is that the distribution of $PCDR$ with height is remarkably narrow and consistent, making this parameter an excellent candidate for chaff identification.

One concern with the generalization of these statistics is that chaff is not released in a systematic way. That is, releases do not seem to correlate spatially, are not released in the same densities or at the same heights, and of course, occur in different atmospheric conditions. As shown in [5], there is certainly a case dependence, so it must be stated that large-scale generalization has risks. However, after years of watching chaff releases on the WSR-88D network, the authors have observed patterns in these releases that are generalizable in, at least, qualitative terms. This is indicated by the similarities in fallout patterns in the 8 cases shown in [5], which was the impetus for the present study. Although

qualitative generalization is helpful, it is assumed that with millions of gates of chaff and hundreds of cases, quantitative generalization is also both possible and helpful. In the case of the data presented in Fig. 6, the discussion in this section presents several theories for why these statistics are physically plausible.

These are generally unsurprising results given previous findings. However, the implications cannot be understated. In a ML algorithm that does not take height (or any spatial considerations) into account, comparing two areas of statistical data at two very different heights could result in the same inference, resulting in an incorrect classification. The findings in this study helped the authors realize the importance of including spatial dimension(s) in ML approaches to classification, as is described in [18] compared to the original approach discussed in [17]. It should also be noted that *generalizations* from a large dataset are necessary for effective ML algorithm training. While these results generally match those from the case studies in [5], case studies are not sufficient to train an expansive algorithm. Discovery of these trends on a larger scale is important for such classification problems.

C. VCP Dependence of Z_H

In searching for additional methods for improving the ML techniques used in [17], the authors noticed that in several cases, the statistics in chaff clouds seemed to change qualitatively when the VCP of the radar changed. This led to the desire to a) quantify these changes, and b) determine the potential applications for algorithm development. As with the importance of spatial statistics mentioned in the previous subsection, changes in statistics by VCP can cause incorrect classifications if not included in training an algorithm. While qualitative statistical changes were observed for several variables, the most quantifiable change with regard to large-scale statistics was seen in the Z_H histograms, which are presented in Fig. 7. The histograms for Z_H are broken into two sets of VCPs: all precipitation VCPs and all clear air VCPs.

Two possible explanations were brought to light during this analysis. First, one of the clear-air VCPs, VCP 31, utilizes a longer pulse, leading to higher sensitivity. However, this higher sensitivity only lowers the minimum detectable Z_H , meaning the noise floor is effectively decreased. If VCP 31 was sufficiently represented in the database, and there were a large number of gates that were below the noise floor of the other VCPs, it would be plausible to think that VCP 31's sensitivity could shift the distributions in this way. A cursory analysis (not shown) of the spatial distribution of chaff clouds in the database combined with an assumed chaff Z_H distribution and the performance metrics of each VCP showed that the shift in distribution was negligible between the scan modes. In fact, the peak did not shift by more than 1 dBZ, leading to the need for another explanation.

It turns out that the database is heavily weighted by clear-air observations, since chaff is *mostly* observed away from weather. One of the hallmarks of clear-air VCPs is that they only scan the lower tilts, leaving the higher tilts out in favor of slower scan speeds while maintaining a respectable volumetric

update rate. When so many cases in the database only contain the lower tilts, one must consider the height-based distributions in Fig. 6 that show decreasing Z_H at lower elevations above radar level. The difference in precipitation versus clear-air VCPs in Fig. 7 are likely a manifestation of the difference in height weighted by the percentage of cases collected in clear-air VCPs.

It should be noted that there can also be other factors biasing the dataset in this manner. We do not consider initial chaff release height, how long it stays in fallout/dispersion, the distribution of heights/ranges versus the available tilts, etc. There are far too many levers to pull that would be potentially better explained by studies directed more at the physical properties of chaff, such as T-matrix calculations. What is important here is that ML algorithms, in their development, training, and testing/validation, must take into account these differences in one way or another. In some cases, the data used in training inherently include these biases; however, in the case of chaff and weather radar, this is another example for the need for spatial data modalities in model training and validation.

V. CONCLUSIONS

In this study, an analysis of statistics in a new database of chaff cases was completed using the WSR-88D weather radar network. A total of 267 cases were used, spanning 71 sites across the contiguous United States (CONUS). This dataset is unique in that it includes an expanded Z_{DR} range from -7.9 – 7.9 dB to -13 – 20 dB. Additionally, several new parameters were investigated that have not yet appeared in the literature, including a proxy for circular depolarization ratio ($PCDR$), an analysis of Z_H , Z_V , Z_{DR} , and $PCDR$ by height, and an analysis of Z_H and Z_{DR} statistics by VCP. The anticipated physical mechanisms for these new observations were discussed, and their relation to algorithm development, especially using ML techniques, was focused upon.

The primary new findings are that Z_{DR} values extend all the way to the edges of the new Z_{DR} range, but there is a wider spread in the histogram at strongly positive values of Z_{DR} , especially between 8 and 13 dB. $PCDR$ values peak at -4 dB, which is close to the value theorized in an adapted $PCDR$ -based model derived from the LDR -based Hertzian dipole model in [16]. However, they trail off toward -20 dB, which indicates expected differences between chaff and true dipoles. The separation relative to hydrometeors is still sufficient to be an excellent separator between chaff and weather, but it is not expected that it will help as much in differentiating chaff from other statistically similar targets such as sea clutter. While the results of Z_H and Z_{DR} distributions with height are not necessarily surprising, they demonstrate the need to include spatial variance in statistical distributions in radar algorithms, especially those that use statistics in clusters with ML techniques. A similar conclusion can be drawn using the VCP findings, which argue that different radar scanning modes should also be included in ML algorithms.

It should be clearly stated that some of the discussion is speculative, without full evidence for the hypotheses stated.

While this may not be fully scientifically satisfying, the hope is that the discussion will spur additional research in these areas, specifically with the thinking that chaff could actually *help* in making new scientific discoveries. A few examples would be investigating PBL structure and electrification using controlled chaff releases, as well as the potential to release chaff nearby supercell thunderstorms in order to examine air motion in and around severe thunderstorms [9].

Moving forward, in the future, the findings in this study should be generalized to other radar systems, processing chains, and operating frequencies. Application of the results in this study to non-WSR-88D radars is recognized as a difficulty, since different radars/frequencies/calibrations could have major effects on the distributions. Generalization would allow for the ability to detect (and possibly filter) chaff across other radar networks. There are multiple ways to accomplish this, including manually collecting chaff cases on other networks/systems, or possibly by conducting T-matrix scattering simulations in order to generalize the polarimetric characteristics of chaff at multiple frequencies. It would also be useful to examine signal-level (I/Q) data within chaff at multiple bands in order to determine any specific spectral characteristics and/or attempt different processing schemes/algorithms.

Finally, it would be prudent to investigate cases of chaff mixed with weather as a specific focus in future work. Although this was not seen often, distributions (and detection) in these cases would be useful to the community. Building a database of these cases would be challenging and would likely need to take place over multiple years (and with more time steps per case) due to their scarcity. However, when chaff is located near weather, its contamination is certainly a problem for weather radar users, making this an interesting area for further exploration.

Specifically, spectral polarimetry is one potential method to separate chaff from weather in a mixed resolution volume. This approach would require I/Q data to explore, which is something that was not readily available for this study. Future I/Q collection in chaff could open the door to exploring this issue, although it is still not expected that clean separation can be achieved since chaff and weather occupy the same Doppler spectral bins (i.e., chaff is a passive tracer).

APPENDIX

DERIVATION OF HERTZIAN DIPOLE MODEL FOR PCDR

Assuming negligible multiple scattering and consistent chaff cut length, the Hertzian dipole model yields [16]:

$$\begin{aligned} \langle |s_{hh}|^2 \rangle &= \langle |f_b|^2 \rangle - \langle (f_b^2 - f_a f_b) A_2 \rangle + \\ &\langle |f_b - f_a|^2 A_4 \rangle \end{aligned} \quad (4a)$$

$$\begin{aligned} \langle |s_{vv}|^2 \rangle &= \langle |f_b|^2 \rangle - 2 \langle (f_b^2 - f_a f_b) A_1 \rangle \\ &+ \langle |f_b - f_a|^2 A_3 \rangle \end{aligned} \quad (4b)$$

$$\begin{aligned} \langle s_{hh}^* s_{vv} \rangle &= \langle |f_b|^2 \rangle + \langle |f_b - f_a|^2 A_5 \rangle \\ &- \langle (f_b - f_a f_b) A_1 \rangle - \langle (f_b^2 - f_a f_b) A_2 \rangle, \end{aligned} \quad (4c)$$

where f_a and f_b are the scattering amplitudes for the electric field along and perpendicular to the dipole axis, respectively. The A_i values are the scattering amplitudes assumed to be fixed with a transverse amplitude of $f_b = 0$. These amplitudes are closed-form solutions for the angular moments as described in Eqs. 2–6 in [16]. Furthermore, if the scattering amplitudes are assumed constant and the transverse component is zero ($f_b = 0$), then (4) reduces to

$$\langle |s_{hh}|^2 \rangle = |f_a|^2 \langle A_4 \rangle \quad (5a)$$

$$\langle |s_{vv}|^2 \rangle = |f_a|^2 \langle A_3 \rangle \quad (5b)$$

$$\langle s_{hh}^* s_{vv} \rangle = |f_a|^2 \langle A_5 \rangle. \quad (5c)$$

Substituting (5) into (2) and (3) yields

$$Z_{DR} = \frac{\langle A_4 \rangle}{\langle A_3 \rangle} \quad (6)$$

and

$$\rho_{HV} = \frac{\langle A_5 \rangle}{\sqrt{\langle A_3 \rangle \langle A_4 \rangle}}. \quad (7)$$

Substituting (6) and (7) into (1) gives

$$PCDR = \frac{A_3 + A_4 - 2A_5}{A_3 + A_4 + 2A_5}. \quad (8)$$

Assuming that the chaff is randomly oriented in the horizontal plane, the radar antenna elevation angle is 0° , and the angle between the chaff axis and horizontal plane is uniformly distributed between 0° and a maximum angle dubbed the flutter angle, [16] derive closed form solutions for angular moments A_i as a function of the flutter angle's complement θ_1 (i.e., the flutter angle is $\pi/2 - \theta_1$, and θ_1 is measured with respect to the true vertical):

$$\langle A_3 \rangle = \frac{1}{5} \cos^4 \theta_1 \quad (9a)$$

$$\langle A_4 \rangle = \frac{3}{40} \left(\sin^4 \theta_1 - \frac{4}{3} \cos^2 \theta_1 + 4 \right) \quad (9b)$$

$$\langle A_5 \rangle = \frac{1}{2} \left(\frac{1}{3} \cos^2 \theta_1 - \frac{1}{5} \cos^4 \theta_1 \right). \quad (9c)$$

ACKNOWLEDGMENT

The authors thank three anonymous reviewers for their helpful comments in revising the original manuscript. This material is based upon work supported by the Observations Program within the NOAA/OAR Weather Program Office under Award No. NA21OAR4590385. Any opinions, findings, conclusions, or recommendations expressed in this material are those of the authors and do not necessarily reflect the views of the National Oceanic and Atmospheric Administration. The authors would like to thank Autumn Millard for her assistance with this work during her internship in the Summer of 2022. Discussions with Earle Williams, David Smalley, Mark

Veillette, David Patterson, Dusan Zrnic, Valery Melnikov, and Alexander Ryzhkov have been exceedingly helpful over the past several years as we continue our desire to learn more about how chaff interacts with weather radar systems.

REFERENCES

- [1] A. D. Martino, *Introduction to Modern EW Systems*. Artech House, 2018.
- [2] T. A. Murphy, R. A. Wade, and B. C. Carcione, "Observations and operational considerations of the 4 June 2013 chaff event in Northern Alabama," *J. Operational Meteorol.*, 2016.
- [3] R. Hessemer, "Scatter communications with radar chaff," *IRE Trans. on Antennas and Propagation*, vol. 9, no. 2, pp. 211–217, 1961.
- [4] C. J. Palermo and L. H. Bauer, "Bistatic scattering cross section of chaff dipoles with application to communications," *Proc. IEEE*, vol. 53, no. 8, pp. 1119–1121, 1965.
- [5] J. M. Kurdzo, E. R. Williams, D. J. Smalley, B. J. Bennett, D. C. Patterson, M. S. Veillette, and M. F. Donovan, "Polarimetric observations of chaff using the WSR-88D network," *J. Appl. Meteor. Climatol.*, vol. 57, no. 5, pp. 1063–1081, 2018.
- [6] E. A. Jessup, "Interpretations of chaff trajectories near a severe thunderstorm," *Mon. Wea. Rev.*, vol. 100, no. 9, pp. 653–661, 1972.
- [7] J. R. Rowland, "Clear air convective behavior revealed by radar chaff," *J. Appl. Meteorol.*, vol. 15, no. 5, pp. 521–526, 1976.
- [8] H. Sauvageot, G. Lafon, and M. Oruba, "Air motion measurements in and around thermal plumes using radar and chaff," *J. Appl. Meteorol.*, vol. 21, no. 5, pp. 656–665, 1982.
- [9] W. R. Moninger and R. A. Kropfli, "A technique to measure entrainment in cloud by dual-polarization radar and chaff," *J. Atmos. Oceanic Technol.*, vol. 4, no. 1, pp. 75–83, 1987.
- [10] R. F. Reinking and B. E. Martner, "Feeder-cell ingestion of seeding aerosol from cloud base determined by tracking radar chaff," *J. Appl. Meteorol.*, vol. 35, no. 9, pp. 1402–1415, 1996.
- [11] E. Jung and B. Albrecht, "Use of radar chaff for studying circulations in and around shallow cumulus clouds," *J. Appl. Meteor. Climatol.*, vol. 53, no. 8, pp. 2058–2071, 2014.
- [12] T. Schuur, A. Ryzhkov, and P. Heinselman, "Observations and classification of echoes with the polarimetric WSR-88D radar," NOAA National Severe Storms Laboratory, Tech. Rep., 2003.
- [13] A. V. Ryzhkov, T. J. Schuur, D. W. Burgess, P. L. Heinselman, S. E. Giangrande, and D. S. Zrnic, "The Joint Polarization Experiment: Polarimetric rainfall measurements and hydrometeor classification," *Bull. Amer. Meteor. Soc.*, vol. 86, no. 6, pp. 809–824, 2005.
- [14] V. M. Melnikov, D. S. Zrnic, R. M. Rabin, and P. Zhang, "Radar polarimetric signatures of fire plumes in Oklahoma," *Geophys. Res. Lett.*, vol. 35, no. 14, 2008.
- [15] D. Klinge-Wilson and J. Evans, "Description of the corridor integrated weather system (CIWS) weather products," MIT Lincoln Laboratory Project Report ATC-317, Tech. Rep., 2005.
- [16] D. S. Zrnic and A. V. Ryzhkov, "Polarimetric properties of chaff," *J. Atmos. Oceanic Technol.*, vol. 21, no. 7, pp. 1017–1024, 2004.
- [17] J. M. Kurdzo, B. J. Bennett, M. S. Veillette, D. J. Smalley, E. R. Williams, and M. F. Donovan, "WSR-88D chaff detection and characterization using an optimized hydrometeor classification algorithm," in *18th Conference on Aviation, Range, and Aerospace Meteorology*, 2017.
- [18] J. M. Kurdzo, B. J. Bennett, M. F. Donovan, and A. L. Millard, "Development and performance of a sea clutter class for the WSR-88D hydrometeor classification algorithm using support vector machines," in *39th Conference on Environmental Information Processing Technologies*, 2023.
- [19] H. S. Park, A. V. Ryzhkov, D. S. Zrnic, and K.-E. Kim, "The hydrometeor classification algorithm for the polarimetric WSR-88D: Description and application to an MCS," *Wea. Forecasting*, vol. 24, no. 3, pp. 730–748, 2009.
- [20] J. M. Kurdzo, B. J. Bennett, D. J. Smalley, and M. F. Donovan, "The WSR-88D inanimate hydrometeor class," *J. Appl. Meteor. Climatol.*, vol. 59, no. 5, pp. 841–858, 2020.
- [21] R. J. Doviak and D. S. Zrnic, *Doppler Radar and Weather Observations*. Dover Publications, 1993.
- [22] A. Ryzhkov, S. Y. Matrosov, V. Melnikov, D. Zrnic, P. Zhang, Q. Cao, M. Knight, C. Simmer, and S. Troemel, "Estimation of depolarization ratio using weather radars with simultaneous transmission/reception," *J. Appl. Meteor. Climatol.*, vol. 56, no. 7, pp. 1797–1816, 2017.
- [23] A. Ryzhkov, P. Zhang, R. Doviak, and C. Kessinger, "Discrimination between weather and sea clutter using Doppler and dual-polarization weather radars," in *URSI General Assembly*, 2002.
- [24] A. Kilambi, F. Fabry, and V. Meunier, "A simple and effective method for separating meteorological from non-meteorological targets using dual-polarization data," *J. Atmos. Oceanic Technol.*, vol. 35, no. 7, pp. 1415–1424, 2018.
- [25] D. Michelson, B. Hansen, D. Jacques, F. Lemay, and P. Rodriguez, "Monitoring the impacts of weather radar data quality control for quantitative application at the continental scale," *Meteorological Applications*, vol. 27, no. 4, 2020.
- [26] A. A. P. Hortal and D. Michelson, "Using a continental-scale data quality monitoring framework to evaluate a new non-weather filter for radar observations," *J. Appl. Meteorol. Climatol.*, 2022.
- [27] A. R. Jameson, "Relations among linear and circular polarization parameters measured in canted hydrometeors," *J. Atmos. Oceanic Tech.*, vol. 4, no. 4, pp. 634–646, 1987.
- [28] D. S. Zrnic, V. M. Melnikov, and J. K. Carter, "Calibrating differential reflectivity on the WSR-88D," *J. Atmos. Oceanic Tech.*, vol. 23, no. 7, pp. 944–951, 2006.
- [29] L. M. Richardson, W. D. Zittel, R. R. Lee, V. M. Melnikov, R. L. Ice, and J. G. Cunningham, "Bragg Scatter Detection by the WSR-88D. Part II: Assessment of ZDR Bias Estimation," *Journal of Atmospheric and Oceanic Technology*, vol. 34, no. 3, pp. 479–493, 2017.



James M. Kurdzo James M. Kurdzo was born in Derby, CT, USA, in 1987. He received the B.S. degree in meteorology from Millersville University, Millersville, PA, USA in 2009, as well as the M.S. degree in meteorology, the M.S. degree in electrical and computer engineering, and the Ph.D. degree in meteorology from the University of Oklahoma, Norman, Oklahoma, USA, in 2011, 2013, and 2015, respectively.

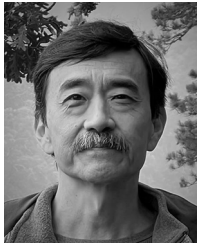
He has been a Technical Staff member at MIT Lincoln Laboratory since 2016, where he is part of the Air Traffic Control Systems Group. He has authored over 30 refereed publications and over 100 conference papers/presentations covering a range of research interests, including radar network and waveform design, severe convective thunderstorms and tornadoes, phased array weather radar technologies, and weather radar algorithms.

Dr. Kurdzo is a senior member of the Institute of Electrical and Electronics Engineers (IEEE) and a member of the American Meteorological Society (AMS). He was a recipient of the MIT Lincoln Laboratory Early Career Technical Achievement award in 2022, the Tommy C. Craighead award for Best Paper in Radar Meteorology (Univ. of Oklahoma) in 2015, and several presentation/paper awards at AMS conferences.



Betty J. Bennett Betty J. Bennett was born in Milwaukee, WI, USA, in 1963. She received the B.S. degree in computer science from Northern Michigan University, Marquette, MI, USA, in 1986. Since joining MIT Lincoln Laboratory in 1988, Betty has worked in a variety of areas with a focus on real-time systems. She is currently a member of the Air Traffic Control Systems Group at Lincoln Laboratory working on the NEXRAD Product Enhancement Team. She has authored or co-authored over 30 refereed articles, technical reports, and conference

papers/presentations.



John Y. N. Cho John Y. N. Cho was born in Tokyo, Japan, in 1963. He received the B.S. and M.S. degrees in electrical engineering from Stanford University, Stanford, CA, USA, in 1985 and 1986, respectively, and the Ph.D. degree in electrical engineering from Cornell University, Ithaca, NY, USA, in 1993.

From 1986 to 1988, he was a U.S. Peace Corps Volunteer in Sierra Leone. From 1993 to 1997, he was a Research Associate at the National Astronomy and Ionosphere Center's Arecibo Observatory, Arecibo, PR, USA. In 1996, he joined the Leibniz Institute for Atmospheric Physics, Kühlungsborn, Germany, as a Visiting Scientist. From 1997 to 2002, he was a Research Scientist with the Department of Earth, Atmospheric, and Planetary Sciences, Massachusetts Institute of Technology, Cambridge, MA, USA. Since 2002, he has been with the MIT Lincoln Laboratory, Lexington, MA, USA, where he is currently a Senior Staff with the Air Traffic Control Systems Group. He has authored or co-authored over 60 refereed articles and over 60 conference papers and technical reports. His research interests include atmospheric radar algorithms, weather sensor benefit quantification, weather effects on air traffic flow management, atmospheric waves and turbulence, noctilucent clouds, and meteors.

Dr. Cho is a member of the American Geophysical Union and the American Meteorological Society. He was a recipient of the CEDAR Prize (NSF), the Young Scientist Award (URSI), and the Best Paper Award (10th USA/Europe ATM R&D Seminar).



Michael F. Donovan Michael F. Donovan was born in Hudson, MA, USA, in 1963. He received the B.S. in meteorology and atmospheric science from University of Massachusetts, Lowell, MA, USA, in 1985. He is currently an Assistant Staff member at MIT Lincoln Laboratory and has been a member of the Air Traffic Control Systems Group since 1987. He has authored or co-authored over 10 refereed articles and over 20 conference papers and technical reports. His research interests include weather radar algorithms, as well as aviation hazards associated

with convective thunderstorms and in-flight icing. He is a member of the American Meteorological Society.